Computational Mechanics 29 (2002) 16–26 © Springer-Verlag 2002
DOI 10.1007/s00466-002-0311-5

Phase transitions in shape memory alloys with hyperbolic heat conduction and differential-algebraic models

R. V. N. Melnik, A. J. Roberts, K. A. Thomas

Abstract The dynamics of phase transitions and hysteresis phenomena in materials with memory are described by a strongly nonlinear coupled system of partial differential equations which, in its generality, can be solved only numerically. Following principles of extended thermodynamics, in this paper we construct a new model for the description of this dynamics based on the Cattaneo–Vernotte law for heat conduction. Models based on the Fourier law follow from this general consideration as special cases. We develop a general procedure for the solution of the resulting systems by their reduction to differential-algebraic systems. Finally, a computational code for the numerical implementation of this procedure is explained in detail, and representative numerical examples are given.

Keywords Phase transitions, Shape memory alloys, Hyperbolic heat conduction

1 Introduction

One of the most difficult problems in computational mechanics is to quantify phase transformations in complex materials. For the so-called "smart" materials this problem is of enormous technological importance. Indeed, performance demands on materials and systems used in engineering applications and infrastructure necessitate the development of such "smart" materials that have the ability to change their properties in response to external and internal stimuli. In this way, new engineering components can be developed leading to improved efficiency and reliability of the whole structure. For many such materials phase transformations and accompanied hysteresis phenomena, demonstrated by the strain–temperature, stress–strain, and stress–temperature relations, are intrinsic parts of the material dynamics. From a mathematical point of view, one of the major difficulties come from the fact that these transformations cannot be characterised by a single-valued function. Indeed, in those solids that do not exhibit structure transitions or plastic deformations, the strain is a single-valued function of stress and temperature, which might not be the case for many "smart" materials exhibiting hysteresis loops. Typical to ferromagnetic, ferroelectric, plasticity effects, such loops arise due to the fact that the underlying process has more than one stable equilibrium. The free energy function for this thermodynamic process should be derived from statistical models, and any physically reasonable approximation of this function will result in a non-convex energy function. In this paper we focus on a specific type of phase transformations, so-called solid–solid phase transformations, in "smart" materials known as shape memory alloys (SMAs). In contrast to ferroelectricity, ferromagnetism, plasticity, where hysteresis phenomena relatively well investigated, this is not the case for pseudoelastic effects that are observed in SMA materials. At the same time, these materials have a huge potential in such fields as electronics, biomedical and environmental engineering, energy production systems, various consumer products, aerospace, and automotive industry, because they can provide functions of sensing, processing, actuation, and feedback [8]. In comparison with other actuating and sensing materials SMAs can offer a number of new important properties such as relatively large reversible strains, high stress, large reversible changes of physical and mechanical characteristics, high damping capacity. However, the adequate modelling of the thermomechanical behaviour of SMAs remains a difficult task due to a strongly nonlinear character of this behaviour including hysteresis loops [1, 6, 10, 24, 33, 39]. Note that the non-convexity of the free energy function "is dictated by the molecular structure of the metallic lattice" which has a highly symmetric phase (austenite) and a less symmetric phase (martensite) capable of twinning [23]. Phase transformations in SMAs are characterised by the deformation which is a result of the crystal-lattice Bain transformations and the lattice-invariant glide/twinning transformations [26]. Such effects as shape memory and pseudo-elasticity are consequences of a martensitic-austenitic phase transition and of twinning in the martensitic phase. Recall that there are three most important categories of phenomena observable in the thermomechanical behaviour of SMAs: (a) *pseudo-elastic effect*, i.e. full recovery in a hysteresis loop upon unloading a large inelastic deformation resulted from loading of a sample;

Received 20 July 2001 / Accepted 5 February 2002

R. V. N. Melnik (✉)
University of Southern Denmark,
Mads Clausen Institute, Sonderborg, DK-6400, Denmark
e-mail: rmelnik@mci.sdu.dk

A. J. Roberts, K. A. Thomas
Department of Mathematics and Computing,
University of Southern Queensland, QLD 4350, Australia

The authors were supported by Australian Research Council small grant 17906.

(b) *shape memory effect*, i.e. full recovery upon heating a large residual deformation after loading-unloading; (c) *thermal hysteresis*, i.e. the ability to recall reversibly and repeatedly both deformed (low temperature) and undeformed (high temperature) shapes when cooled and heated at a constant load (e.g., [5]). Our goal in this paper is to construct a computational procedure which is able to give an adequate description of these effects. Solid–solid martensitic phase transformations in SMA materials are produced by nucleation and growth, and they are thought as "diffusionless" referring to a process for which each atom moves a distance less than an atomic distance. The models considered here can be treated as a link between microscopic and macroscopic types of models. They are often termed as mesoscopic models due to the fact that their basic element is a small part of the metallic lattice that forms the body, sometimes called the lattice "particle" or "cell" [23]. To put it differently, we aim at quantifying phenomena that take place at the mesoscale ($\sim\mu$m) or smaller with models describing the material behaviour at the macroscopic scale ($\sim$cm) [5]. The model and the algorithm developed in this paper provide a basis for the analysis of the dynamics of phase transitions in shape memory alloys (SMA) for various types of dynamic loadings, and due to this fact the results reported here might prove to be useful in related areas of research, including modelling of SMA-based composites [7].

We structure our further discussion in the following way. In Sect. 2 we discuss mechanisms for thermomechanical coupling in models describing SMA dynamics and formulate the model used as the basis for our analysis in this paper. In Sects. 3 and 4 we give details of constitutive relations, and in Sect. 5 we formulate a complete model for the dynamics of phase transitions in a SMA rod. Section 6 is devoted to the description of a reduction procedure of our model to a system of differential-algebraic equations, and in Sect. 7 we give representative examples of our computational experiments. In Sect. 8 we make concluding remarks, and discuss future directions of the presented work.

2
Nonlocal coupled models of nonlinear thermoelasticity

Consider a 3D SMA sample that occupies the volume V in a fixed reference spatial configuration Ω at a certain time t_0. Let further $\rho_0(\mathbf{x}, t_0) > 0$ be the density of the SMA sample (the mass per unit volume) in the reference configuration Ω at time t_0 and $\rho(\mathbf{x}, t)$ be the density of the matter at time t where $t - t_0$ is sufficiently small. Before we proceed to balance equations for the description of the dynamic thermomechanical behaviour of the sample under quite general loading conditions, we need information on forces acting per unit area of the sample. This brings along the concept of stresses, which in contrary to what is often assumed, cannot be defined here by a mere function of the deformation gradient. It is essential for us to note that stresses also depend on temperature of the sample, its rate of change in time, and the rate of change of deformation gradient $\boldsymbol{\epsilon}$. In the general case deformation gradient $\boldsymbol{\epsilon}$ is a nonlinear function, and in some SMA applications the inelastic strain might not be small, and some results are available in the framework of finite-strain theory [2]. However, the strain linearisation hypothesis has proved to be plausible in a range of SMA application areas [1, 22, 28, 33, 34], and we follow this assumption in this paper. In particular, we identify the partial derivative of displacement $\mathbf{u} = (u_1, u_2, u_3)$ with respect to $\mathbf{x} = (x_1, x_2, x_3)$ (material or Lagrangian coordinates of a material point of the sample in the configuration Ω at time t_0) with the symmetric strain tensor

$$\boldsymbol{\epsilon} = \mathrm{sym}\left[\frac{\partial \mathbf{u}(\mathbf{x}, t)}{\partial \mathbf{x}}\right] \quad \text{or}$$
$$\epsilon_{ij}(\mathbf{x}, t) = \frac{1}{2}\left[\frac{\partial u_i(\mathbf{x}, t)}{\partial x_j} + \frac{\partial u_j(\mathbf{x}, t)}{\partial x_i}\right], \quad i, j = 1, 2, 3 \ , \tag{1}$$

where we require that $\det(\mathbf{I} + \boldsymbol{\epsilon}) > 0$ which precludes a possibility of compression of the sample matter to zero and guarantees the local invertibility of $\mathbf{x} + \mathbf{u}(\mathbf{x}, t)$ [35]. Since the time derivatives are understood in the Lagrangian sense, $\mathbf{x}$ is kept fixed in (1). Now we are in a position to proceed with a general formulation of balance law equations.

1. In the Lagrangian system of coordinates $(\mathbf{x}, t)$, the equation for balance of mass is written in the form [35]

$$\rho(\mathbf{x}, t)\det(\mathbf{I} + \boldsymbol{\epsilon}(\mathbf{x}, t)) = \rho_0(\mathbf{x}, t_0) \ . \tag{2}$$

2. The equation of motion has the following form

$$\rho \frac{\partial^2 \mathbf{u}}{\partial t^2} = \nabla_{\mathbf{x}} \cdot \mathbf{s} + \mathbf{F} \quad \text{with } \mathbf{F} = \rho(\mathbf{f} + \hat{\mathbf{f}}) - \hat{\rho}\mathbf{v} \ , \tag{3}$$

where $\mathbf{f}$ is a given body force per unit mass, $\hat{\rho}$ and $\hat{\mathbf{f}}$ are nonlocal mass and force residuals respectively, and $\mathbf{s}$ is the stress tensor.

3. Finally, in Lagrangian coordinates the equation for energy balance has the form

$$\rho \frac{\partial}{\partial t}\left(e + \frac{\mathbf{v}^2}{2}\right) - \nabla_{\mathbf{x}} \cdot (\mathbf{s} \cdot \mathbf{v}) + \nabla \cdot \mathbf{q} = \rho\left(h + \hat{h} + \mathbf{f} \cdot \mathbf{v} - \frac{\hat{\rho}}{\rho}\left(e + \frac{\mathbf{v}^2}{2}\right)\right) \ , \tag{4}$$

where e is the internal energy (per unit mass) of the system, $\mathbf{v}^2 = \mathbf{v} \cdot \mathbf{v}$, $\mathbf{v} = \partial \mathbf{u}/\partial t$ (that is $v_i(\mathbf{x}, t) = \partial u_i(\mathbf{x}, t)/\partial t$, $i = 1, 2, 3$), h is the heat source density, $\hat{h}$ is the nonlocal energy residual (see [3] for conditions on localised residuals) and $\mathbf{q}$ is the heat flux.

As a next step, we note that the scalar multiplication of (3) by $\mathbf{v}$ gives

$$\rho \frac{\partial \mathbf{v}^2/2}{\partial t} - \mathbf{v} \cdot (\nabla \cdot \mathbf{s}) = (\mathbf{F}, \mathbf{v}) \equiv \rho(\mathbf{f} + \hat{\mathbf{f}}) \cdot \mathbf{v} - \hat{\rho}\mathbf{v}^2 \ . \tag{5}$$

Taking into account normalisation, from (4) and (5) we get

$$\rho \frac{\partial e}{\partial t} - \mathbf{s}^T : (\nabla \mathbf{v}) + \nabla \cdot \mathbf{q} = g \ , \tag{6}$$

where $\mathbf{a}^T : \mathbf{b} = \sum_{i,j=1}^{3} a_{ij} b_{ij}$ is the standard notation, given the rank 2 tensors $\mathbf{a}$ and $\mathbf{b}$, and

$$g = \rho(h + \hat{h}) - \rho\hat{\mathbf{f}} \cdot \mathbf{v} - \hat{\rho}\left(e - \frac{\mathbf{v}^2}{2}\right) \ . \tag{7}$$

The right-hand sides of Eqs. (3) and (6) incorporate into the model *nonlocal and dissipative effects of thermomechanical waves*. Moreover, as we shall see in the next section, under appropriate constitutive relations it is also possible to allow for a relaxation time for acceleration of the motion in response to applied gradients such as the deformation gradient and the temperature gradient.

We assume that there exists a one-to-one entropy function of the system state. We denote the density of such a function by η, and then the second law of thermodynamics is

$$\frac{\partial \eta}{\partial t} - \nabla \cdot \mathbf{r} \geq \xi + \hat{\xi} - \frac{\hat{\rho}}{\rho} \ , \tag{8}$$

where ξ is the entropy source density, $\mathbf{r}$ is the entropy flux density and $\hat{\xi}$ is the nonlocal entropy residual.

The system of equations (3), (6) combined with inequality (8) provides the general mathematical model for the description of thermomechanical behaviour of dynamic systems. The macroscopic modelling of such systems starts from the choice of constitutive relationships. We assume the existence of a functional Ψ invariant under a time shift and chose this functional in the form of the Helmholtz free energy

$$\Psi = e - \theta\eta \ , \tag{9}$$

where θ is the temperature of the system ($\theta > 0$, $\inf_{(\mathbf{x},t)} \theta = 0$). We also assume specific forms for the entropy flux and the entropy source density as

$$\mathbf{r} = \mathbf{q}/\theta, \quad \xi = h/\theta \ . \tag{10}$$

Using (9) in (6) and taking into account that

$$\nabla \cdot \mathbf{q} = \theta \nabla \cdot (\mathbf{q}/\theta) + (\mathbf{q} \cdot \nabla\theta)/\theta \ , \tag{11}$$

from (8) and (10) we get the nonlocal formulation of the Clausius–Duhem inequality

$$-\frac{\hat{\rho}}{\rho}\left(\Psi - \frac{\mathbf{v}^2}{2}\right) - \left(\frac{\partial \Psi}{\partial t} + \eta\frac{\partial \theta}{\partial t}\right) + \mathbf{s}^T : \nabla\mathbf{v} - \hat{\mathbf{f}} \cdot \mathbf{v} - \frac{\mathbf{q} \cdot \nabla\theta}{\theta} - (\theta\hat{\xi} - \hat{h}) \geq 0 \ . \tag{12}$$

The latter inequality together with requirements on localisation residuals (see [3] for details) impose restrictions on the choice of nonlocal residuals and the functions η, $\mathbf{s}$ and $\mathbf{q}$. We assume that the entropy density is given in the form

$$\eta = -\frac{\partial \Psi}{\partial \theta} \ . \tag{13}$$

Finally, we have to specify the constitutive relationships that couple stresses, deformation gradients, temperature and heat fluxes

$$\Phi_1(\mathbf{s}, \boldsymbol{\epsilon}) = 0, \quad \Phi_2(\mathbf{q}, \theta) = 0 \ , \tag{14}$$

where it is implicitly assumed that these relations may involve spatial and temporal derivatives of the functions. In next sections we specify particular forms for Φ_1 and Φ_2 used in our computational experiments.

3
The Cattaneo–Vernotte model for heat conduction

The function Φ_2 in (14) is chosen on the basis of the principles of extended thermodynamics [32] by using the Cattaneo–Vernotte model for heat conduction

$$\mathbf{q} + \tau_0 \frac{\partial \mathbf{q}}{\partial t} = -k(\theta, \boldsymbol{\epsilon})\nabla\theta \ , \tag{15}$$

where τ_0 is the dimensionless thermal relaxation time and $k(\theta, \boldsymbol{\epsilon})$ is the thermal conductivity of the material (typically $k = 1 + \tilde{\beta}\theta$ with the given dimensionless coefficient $\tilde{\beta}$). Incorporating this model into the general description of thermomechanics of SMA materials allows one to account for the finite speeds of thermal wave propagation and thermally induced stress wave propagation coupled to the deformation gradient (see also [41] and references therein). Although the interest to hyperbolic approaches in the analysis of materials with memory has increased (e.g., [14]) in such a generality as it is proposed in the present paper the dynamic behaviour of SMA materials has not been modelled before.

In order to incorporate Eq. (15) into our general model of thermoelasticity we use a consequence of (6)

$$\rho\tau_0 \frac{\partial^2 e}{\partial t^2} - \tau_0 \frac{\partial}{\partial t}[\mathbf{s}^T : (\nabla\mathbf{v})] + \tau_0 \nabla \cdot \left(\frac{\partial \mathbf{q}}{\partial t}\right) = \tau_0 \frac{\partial g}{\partial t} \ . \tag{16}$$

On the other hand, from (15) we get

$$\nabla \cdot \mathbf{q} + \tau_0 \nabla \cdot \left(\frac{\partial \mathbf{q}}{\partial t}\right) = -\nabla \cdot (k\nabla\theta) \ . \tag{17}$$

Then from (6), (16), (17) we obtain the energy balance equation in the form

$$\rho\frac{\partial e}{\partial t} + \rho\tau_0 \frac{\partial^2 e}{\partial t^2} - \mathbf{s}^T : (\nabla\mathbf{v}) - \tau_0 \frac{\partial}{\partial t}[\mathbf{s}^T : (\nabla\mathbf{v})] - \nabla \cdot (k\nabla\theta) = G \ , \tag{18}$$

where $G = g + \tau_0(\partial g/\partial t)$.

4
The Landau–Devonshire model for the Helmholtz free energy and the stress–strain relation

Temperature is a key component in the dynamics of shape-memory-alloys, and changing thermal conditions SMA materials can exhibit qualitatively different behaviours. As it has been observed experimentally, *ferroelastic*, *pseudoelastic*, and *elastic* like behaviours of SMA samples are expected for low, intermediate, and high temperatures, respectively [16]. Such a wide range of qualitatively different behaviours can be adequately described only if the thermal and mechanical fields are considered in an intrinsic coupling. This coupling in mathematical models can be accounted for by an appropriate choice of the free energy function. A "slight" change in this function (such as the account for [or omitting of] the viscous or coupled stresses, thermal memory terms, etc. [39]) may require completely different mathematical arguments in the analysis of the well-posedness of the model and in the construction of numerical schemes for its solution.

Having computational experiments in mind, our further discussion is focused on the one-dimensional case assuming the following approximation for the free energy of the system

$$\Psi(\theta,\epsilon) = \psi_0(\theta) + \psi_1(\theta)\psi_2(\epsilon) + \psi_3(\epsilon) \tag{19}$$

where $\psi_0(\theta)$ models thermal field contributions, $\psi_1(\theta)\psi_2(\epsilon)$ models shape-memory contributions and $\psi_3(\epsilon)$ models mechanical field contributions. Note that although the material laws are inherently multidimensional, on a number of occasions a reduction in dimensionality is possible. In this paper we consider a SMA wire/rod, but our procedure can be extended to the multidimensional case and some key ideas of such an extension have been already discussed in [28]. Our considerations here are based on the following forms of functions ψ_m, $m = 0, 1, 2, 3$

$$\begin{aligned}&\psi_0(\theta) = \alpha_0 - \alpha_1\theta\ln\theta, \quad \psi_1(\theta) = (1/2)\alpha_2\theta, \quad \psi_2(\epsilon) = \epsilon^2,\\ &\psi_3(\epsilon) = -(1/2)\alpha_2\theta_1\epsilon^2 - (1/4)\alpha_4\epsilon^4 + (1/6)\alpha_6\epsilon^6\ ,\end{aligned} \tag{20}$$

where all α_i and θ_1 are positive constants. Some authors include a linear term $\alpha^0\theta$ into $\psi_0(\theta)$. Since this term has no bearing on the final model and changes only the value of the coefficient of θ in the internal energy representation (see formula (25)), it is omitted in our consideration. The model (19)–(20), known as the Landau–Devonshire model for the Helmholtz free energy [16, 17], covers a number of important practical cases. However, it belongs to the class of models which is difficult to investigate compared to the Landau–Devonshire–Ginzburg model. In the latter case an additional "smoothing" term, γu_{xxxx}, appears in (19)–(20). This term, known as the the Ginzburg term, is due to the extra term in the approximation of the free energy function (coupled stress $\zeta = \zeta(\epsilon_x)$). This term is sometimes brought into consideration by assuming the dependency of the free energy on a change of the curvature ϵ_x of the metallic lattice. From a mathematical point of view, it simplifies the analysis of the model by allowing us to obtain a bound of the deformation gradient (strain) using a well established technique [13]. We do not proceed with such an analysis here. However, we note that one has to realise that the models under consideration (the Landau–Devonshire and Landau–Devonshire–Ginzburg models) provide just two good examples of many possible approximations of the free energy function.

We analysed both these models numerically. Unfortunately, the definition of the Ginzburg term varies in the literature, but in those cases where $\zeta = (\gamma/2)\epsilon_x^2$ reported values of γ ($\gamma \sim 10^{-10}$–10^{-12}) showed little influence on the dynamics of shape-memory alloys in all computational experiments we have performed so far (see also [28]). Having said that, we should mention that there is evidence to suggest that for the deformation-driven set of computational experiments the choice of the value for the Ginzburg coefficient can help in differentiating between rate-dependent and rate-independent hystereses (e.g., [11] and references therein). Moreover, a number of important characteristics of phase transformations (such as the size of hysteresis) may depend on the contributions of the interfacial energies, and these contributions can often be approximated with the Ginzburg correction term. Nevertheless, the Ginzburg coefficient can only be determined in approximate order [40] and in the general case this coefficient may not be temperature-independent. So, further experimental results are needed to clarify this issue further.

The choice of the function Ψ in (9), and consequently in (19)–(20), brings major difficulties in the investigation of the model. Strictly speaking, the free energy function strongly depends upon the statistics of the phenomenon and has to be derived from a statistical model. Since van der Waals work on statistical mechanics it is a common practice to choose this function as a non-convex function of $\boldsymbol{\epsilon}$ [23]. When dealing with shape memory alloys, minima of this function are known to correspond different phases of the material. For example, in the case of three minima, we expect one austenitic and two martensitic phase (see, for example, [16, 20, 40]). Temperature plays a crucial role in the phase transition. Depending on the value of temperature, the material may alternate between a single thermodynamically unstable nonmonotone branch and multiple unstable branches. The character of this instability depends not only on the deformation gradient and temperature, but also on the rates of their changes.

As for other possible definitions of the free energy function we mention an approach of taking into account the contributions of interfacial energies by assuming [9, 31]

$$\Psi = (1-z)\tilde{\psi}_1(\epsilon,\theta) + z\tilde{\psi}_2(\epsilon,\theta) + z(1-z)\tilde{\psi}_3\ , \tag{21}$$

where z is the volume fraction of martensite (i.e. the product phase), $(1-z)$ is the volume fraction of austenite (i.e. the parent phase), $\tilde{\psi}_1$, $\tilde{\psi}_2$ are the free energies of austenite and martensite respectively and $\tilde{\psi}_3$ is the contribution from the interaction effect between austenite and martensite. This representation can be implemented into our numerical scheme, if required.

Having defined the free energy function, we can discuss approximations of constitutive models. First, we note that in the general case the choice of the function Φ_1 in (14) should be made having in mind the dependency of the stress on the rate of temperature and the deformation gradient, e.g.

$$s = \rho\left[p(\theta,\epsilon) + \lambda\left(\frac{\partial\theta}{\partial t}, \frac{\partial\epsilon}{\partial t}\right)\right]\ , \tag{22}$$

where

$$p(\theta,\epsilon) = \frac{\partial\Psi}{\partial\epsilon}, \quad \lambda\left(\frac{\partial\theta}{\partial t}, \frac{\partial\epsilon}{\partial t}\right) = \tilde{\mu}(\theta)\frac{\partial\epsilon}{\partial t} + \tilde{\nu}(\epsilon)\frac{\partial\theta}{\partial t}\ .$$

Then, it is straightforward to deduce

$$p(\theta,\epsilon) = \alpha_2\theta\epsilon + \frac{\partial\psi_3(\epsilon)}{\partial\epsilon} = \left[\alpha_2\epsilon(\theta-\theta_1) - \alpha_4\epsilon^3 + \alpha_6\epsilon^5\right]\ . \tag{23}$$

Note that the minimisation of nonconvex functionals such as (19)–(20) arises frequently in material science applications, and structural phase transitions in crystalline solids can often be modelled effectively with nonconvex variational problems [25]. In particular, we have to deal

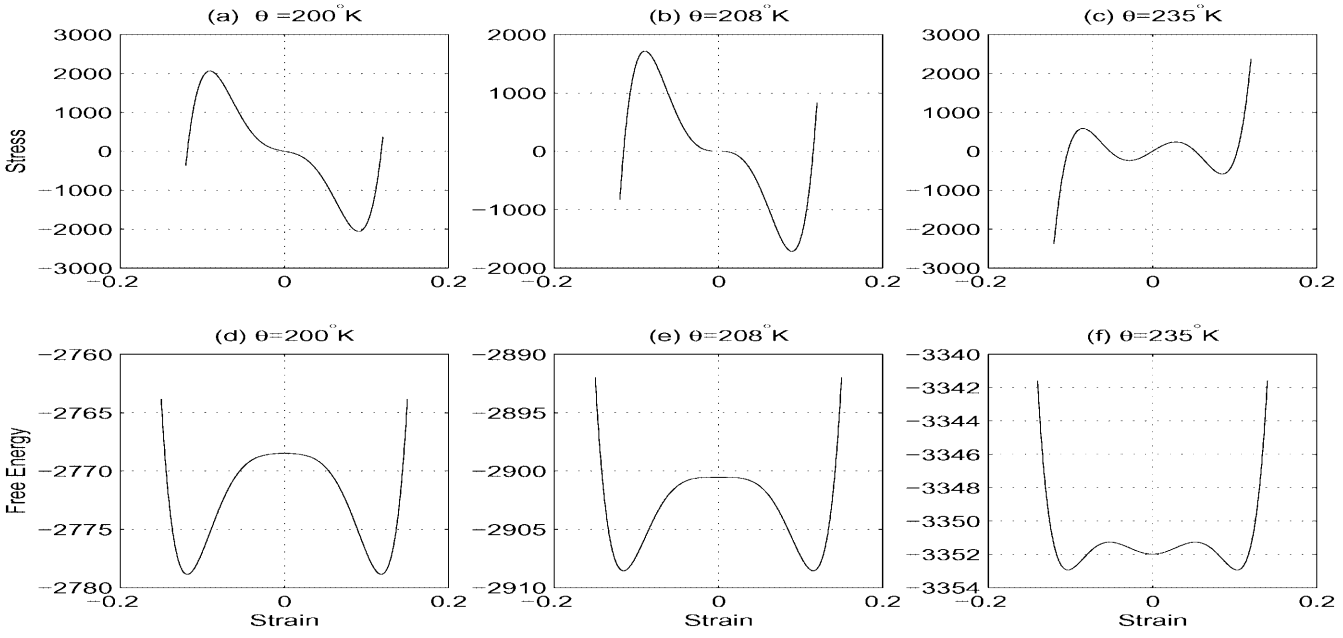

Fig. 1. Modelling the transition from "elastoplastic" to "quasiplastic" state

with nonconvex free energy functions in those cases where the material exhibits microstructures in which the deformation gradient oscillates on "infinitesimal" scale between two symmetry-related variants of the martensitic phase. Depending on the type of transformation (cubic-to-orthorhombic, cubic-to-monoclinic, or cubic-to-tetragonal) we have to deal with distinctively different dynamic behaviour of the material [19].

The basic idea of this approach in the context of modelling shape-memory alloys was initiated in [16] and we demonstrate this idea in Figs. 1–3 for the material $Au_{23}Cu_{30}Zn_{47}$ where the free energy and the stress are depicted as functions of strain. Although the free energy function depends on the statistics of the phenomenon, in many shape-memory alloy applications it can be sufficiently well approximated by a non-convex function such as (19)–(20). Minima of this function are known to correspond different phases of the material, and depending on the value of temperature, the material may alternate between a single thermodynamically unstable nonmonotone branch and multiple unstable branches. In particular, in the low temperature range (see Fig. 1), one observes

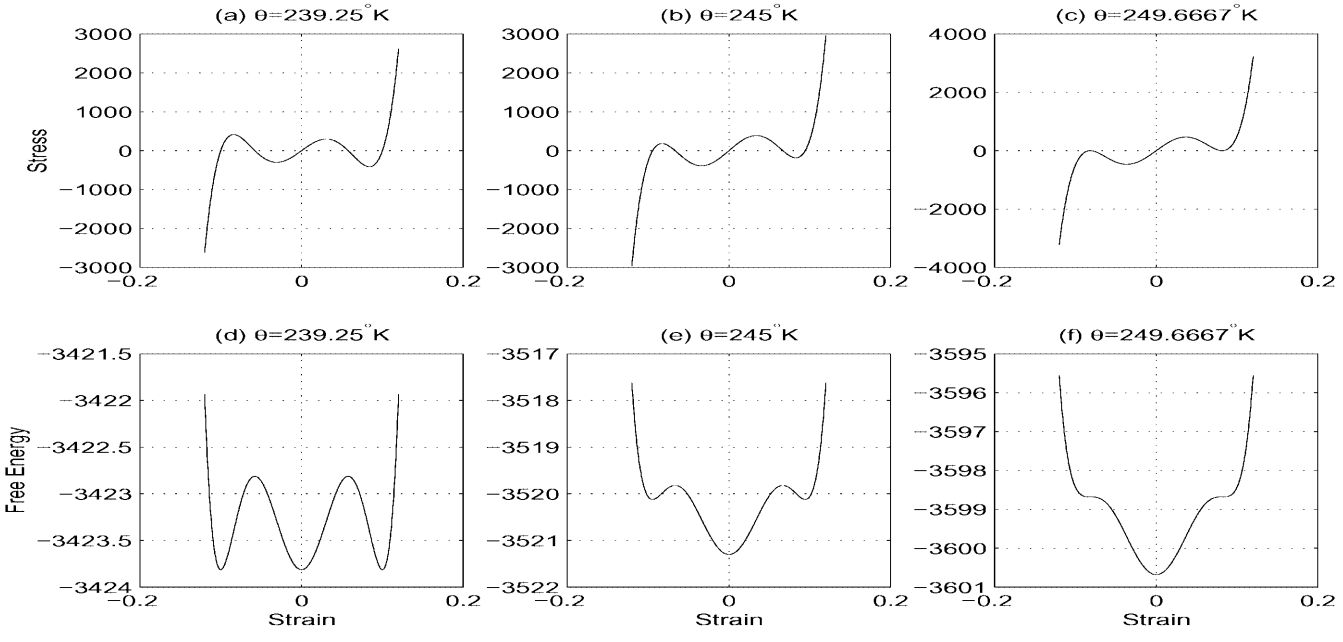

Fig. 2. Modelling the transition from "quasiplastic" to "pseudoelastic" state

that martensite twins (represented by two minima of the free energy function) prevail. When the temperature increases, initially "elastoplastic" (or ferroelastic) material exhibits a "quasiplastic" behaviour where one observes that austenite and martensite twins phases co-exist (see Fig. 2). By increasing temperature further, the behaviour of the material becomes "pseudoelastic" with the prevailing austenite phase (see Fig. 3). Finally, the material returns to its "almost-elastic" state by completing a hysteresis loop. The approximations described above provide a good agreement with experimental isothermal load-deformation curves reported in the literature [16, 21]. Our computational experiments show that these approximations allow us to reproduce adequately the main nonlinear effects characterising the dynamic behaviour of the material in the first order solid-solid phase transitions. Nevertheless, a complex character of thermomechanical coupling in SMA materials requires the development of new refined approximations to constitutive models (14) [15, 38]. It should be emphasised that it is conceptually straightforward to incorporate refined constitutive models into computational schemes proposed here.

5
One-dimensional hyperbolic approximation of shape-memory-alloy dynamics and coupling mechanisms for thermomechanical dynamics

Using the model (19) and (20), from (13) we get

$$\eta = \alpha_1(1 + \ln\,\theta) - (1/2)\alpha_2\epsilon^2 \ . \tag{24}$$

This enables us to find the internal energy of the system as a sum of thermal and mechanical fields contributions

$$\begin{aligned} e &= \alpha_0 + \alpha_1\theta - (1/2)\alpha_2\theta_1\epsilon^2 - (1/4)\alpha_4\epsilon^4 + (1/6)\alpha_6\epsilon^6 \\ &= \alpha_0 + \alpha_1\theta + \psi_3(\epsilon) \ . \end{aligned} \tag{25}$$

The substitution of (25) into (18) leads to the final form of the energy balance equation. In particular, assuming symmetry of the deformation gradient tensor, we get

$$\rho\alpha_1\left[\frac{\partial\theta}{\partial t} + \tau_0\frac{\partial^2\theta}{\partial t^2}\right] + A(\epsilon,\theta) - \nabla\cdot(k\nabla\theta) = G \ , \tag{26}$$

where the meaning of A is

$$\begin{aligned} A(\epsilon,\theta) = &-\rho\alpha_2\left\{\theta\epsilon\frac{\partial\epsilon}{\partial t} + \tau_0\frac{\partial}{\partial t}\left[\theta\epsilon\frac{\partial\epsilon}{\partial t}\right]\right\} \\ &- \rho\tilde{\mu}(\theta)\left\{\left(\frac{\partial\epsilon}{\partial t}\right)^2 + \tau_0\frac{\partial}{\partial t}\left[\left(\frac{\partial\epsilon}{\partial t}\right)^2\right]\right\} \\ &- \rho\frac{\partial\theta}{\partial t}\left\{\tilde{v}(\epsilon)\frac{\partial\epsilon}{\partial t} + \tau_0\frac{\partial}{\partial t}\left[\tilde{v}(\epsilon)\frac{\partial\epsilon}{\partial t}\right]\right\} \ . \end{aligned} \tag{27}$$

Equation (26) is solved together with the equation of motion (3) with respect to (u,θ):

$$\begin{aligned} &C_v\left[\frac{\partial\theta}{\partial t} + \tau_0\frac{\partial^2\theta}{\partial t^2}\right] - k_1\left[\theta\frac{\partial u}{\partial x}\frac{\partial^2 u}{\partial t\partial x} + \tau_0\frac{\partial}{\partial t}\left(\theta\frac{\partial u}{\partial x}\frac{\partial^2 u}{\partial t\partial x}\right)\right] \\ &\quad - \mu\left[\left(\frac{\partial^2 u}{\partial t\partial x}\right)^2 + \tau_0\frac{\partial}{\partial t}\left(\frac{\partial^2 u}{\partial t\partial x}\right)^2\right] \\ &\quad - \nu\left[\frac{\partial\theta}{\partial t}\frac{\partial^2 u}{\partial t\partial x} + \tau_0\frac{\partial}{\partial t}\left(\frac{\partial\theta}{\partial t}\frac{\partial^2 u}{\partial t\partial x}\right)\right] - \frac{\partial}{\partial x}\left(k\frac{\partial\theta}{\partial x}\right) = G, \\ &\rho\frac{\partial^2 u}{\partial t^2} - \frac{\partial}{\partial x}\left[k_1\frac{\partial u}{\partial x}(\theta-\theta_1) - k_2\left(\frac{\partial u}{\partial x}\right)^3 + k_3\left(\frac{\partial u}{\partial x}\right)^5\right] \\ &\quad - \mu\frac{\partial^3 u}{\partial x^2\partial t} - \nu\frac{\partial^2\theta}{\partial x\partial t} = F \ , \end{aligned} \tag{28}$$

where F is the one-dimensional analogue of function $\mathbf{F}$ defined in Sect. 2, and $C_v = \rho\alpha_1$, $k_1 = \rho\alpha_2$, $k_2 = \rho\alpha_4$, $k_3 = \rho\alpha_6$, $\mu = \rho\tilde{\mu}$, $\nu = \rho\tilde{\nu}$.

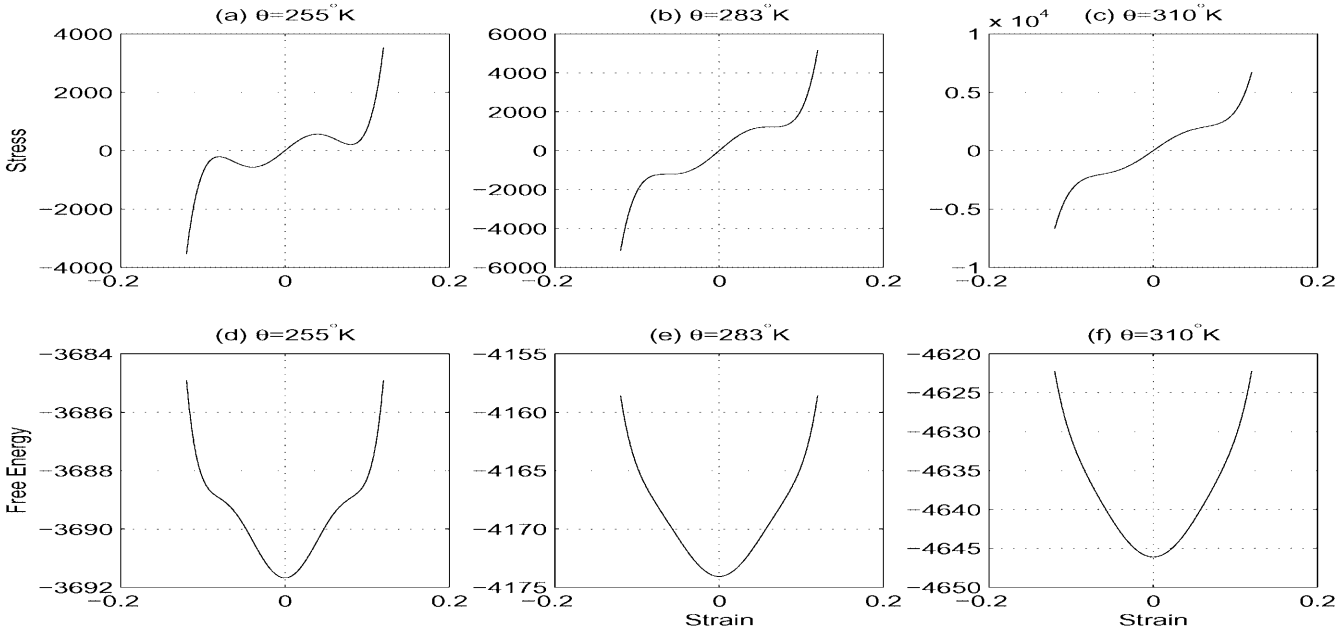

Fig. 3. Modelling the transition from "pseudoelastic" to "almost-elastic" state

The initial conditions for the model (28) are chosen in the form

$$u(x,0) = u^0(x), \quad \frac{\partial u}{\partial t}(x,0) = u^1(x); \qquad \theta(x,0) = \theta^0(x), \quad \frac{\partial \theta}{\partial t}(x,0) = \theta^1(x) \ , \tag{29}$$

for given functions u^0, u^1, θ^0, θ^1. There are several distinct choices for boundary conditions to be used in our computational experiments. Mechanical boundary conditions are taken in one of the following forms (L is the length of the structure):

- "stress-free" boundary conditions: $s(0,t) = s(L,t) = 0$;
- "pinned end" boundary conditions: $u(0,t) = u(L,t) = 0$;
- or mixed mechanical boundary condition: $s(0,t) = 0$, $u(L,t) = 0$.

When displacements are given on boundaries, a priori bounds on strains are generally unknown which complicates the mathematical analysis of the problem. Our computational code can treat easily this situation, and we present a representative example in Sect. 7. Thermal boundary conditions are chosen in one of the following form

- "thermal insulation" boundary conditions: $q(0,t) = q(L,t) = 0$, which reduce to $(\partial\theta/\partial x)(0,t) = (\partial\theta/\partial x)(L,t) = 0$ for the Fourier law;
- "controlled flux" boundary conditions: $(\partial\theta/\partial x)(0,t) = 0$, $-k(\partial\theta/\partial x)(L,t) = \beta[\theta - \theta^0(t)]$;
- or fixed temperature ("uncontrolled energy flow") boundary conditions: $\theta(0,t) = \theta(L,t) = 0$.

In the last case additional assumptions are needed. By using the Leray–Schauder principle and the Lumer–Phillips theorem, the Cauchy problem for nonlinear hyperbolic model of thermoviscoelasticity (28) can be analysed with a technique developed in [13].

6 Computational methodology for SMA modelling based on reductions to differential-algebraic systems

Consider system (28). The major difficulty in the numerical solution of this system is coming from terms responsible for the coupling phenomenon, in particular from $k_1\theta(\partial u/\partial x)(\partial v/\partial x)$ and $(\partial/\partial x)(k_1(\partial u/\partial x)(\theta - \theta_1))$ in the first and the second equation, respectively. Therefore, in explaining our numerical procedure we concentrate on a simplified version of the model by assuming $\tau_0 = \mu = \nu = 0$. The procedure is generalised to the case (28) in a straightforward manner. Our basic idea is to reduce the model to a system of differential-algebraic equations. It is clear that the thermomechanical behaviour of SMA materials is fairly complicated, and thermodynamic constitutive equations will be continuously re-examined by the researchers as new experimental data becomes available. It is advantageous therefore to consider the stress-strain relationship as a separate algebraic equation rather than to substitute it into the coupled system of balance equations for momentum and energy. Indeed, our model under the conditions specified above can be reduced to

$$R\frac{\partial \mathbf{c}}{\partial t} = \mathbf{a}, \qquad s = k_1(\theta - \theta_1)\frac{\partial u}{\partial x} - k_2\left(\frac{\partial u}{\partial x}\right)^3 + k_3\left(\frac{\partial u}{\partial x}\right)^5 \tag{30}$$

where $R = \mathrm{diag}(1, \rho, C_v)$, $\mathbf{c} = (u, v, \theta)^{\mathrm{T}}$, $\mathbf{a} = (v, \partial s/\partial x + F, k\partial^2\theta/\partial x^2 + k_1\theta(\partial u/\partial x)(\partial v/\partial x) + G)^{\mathrm{T}}$. The system (30) should be solved with respect to (u, v, θ, s). It is this system that was used for our computational experiments reported in the next section. Similar systems can be derived for other dynamic models describing the coupled thermomechanical behaviour of SMA materials. Note that the term $\partial u/\partial x = \epsilon$ in (30) is the linearised strain that plays the role of the order parameter in the Landau theory. The initial and boundary conditions for this model are problem-specific, as we discussed in Sect. 5. Our computational experiments presented in the next section deal with a copper-based alloy $Au_{23}Cu_{30}Zn_{47}$ (see Figs. 1–3). We consider a rod of the length $L = 1$ cm with the following physical parameters $k = 1.9 \times 10^{-2}$ cm g/(ms^3 K), $\rho = 11.1$ g/cm^3, $C_v = 29$ g/(ms^2 cm K), $\theta_1 = 208$ K, $k_1 = 480$ g/(ms^2 cm K), $k_2 = 6 \times 10^6$ g/(ms^2 cm K), $k_3 = 4.5 \times 10^8$ g/(ms^2 cm K) (e.g., [16, 33] for further details on this materials and [28] on copper-based SMAs in general).

Previously developed numerical procedures are usually based on finite element algorithms (e.g., [22, 33]), and are not easily tailored to new and improved constitutive relations. The approach we propose here is different from those previously reported. First, we reduce the original PDE model to a system of differential-algebraic equations in a way similar to that of (30). Then, we use one of the backward difference integration algorithms developed by us in MATLAB. Let us explain the algorithm applied in some detail. Similar to such codes as DASSL and their further developments, e.g., DSL48S, we want to solve numerically initial value problems for differential-algebraic equations in the general form [18]

$$\tilde{\boldsymbol{f}}(\dot{\boldsymbol{y}}, \boldsymbol{y}, t) = \boldsymbol{0}, \quad \boldsymbol{y}, \dot{\boldsymbol{y}} \in R^m \ . \tag{31}$$

In (31) $\tilde{\boldsymbol{f}}$ is a map $R^m \times R^m \times R^m \to R^m$, and in the general case the Jacobian $\partial\tilde{\boldsymbol{f}}/\partial\dot{\boldsymbol{y}}$ is singular, which requires the development novel procedures compared to ordinary differential equations. As a special case, stiff systems of ODEs can also be treated with our code.

We follow [37] in describing the algorithm. For simplicity, we explain the basic steps on an example of a linear system of DAEs in the form $M\mathrm{d}\boldsymbol{y}/\mathrm{d}t = \tilde{\boldsymbol{f}}(t) + K\boldsymbol{y}$, where M and K are (typically sparse) matrices obtained from spatial discretisations of a PDE equation or a system ($\boldsymbol{y} \in R^m$ is a vector to be found). If M is close to singular, the DAE can be solved by using a methodology for numerical solution of stiff ODE. In particular, we can start with an implicit Euler-like schemes $M(\boldsymbol{y}_{n+1} - \boldsymbol{y}_n)/h = \boldsymbol{f}(t+h) + K\boldsymbol{y}_{n+1}$. For the unforced dynamics we have $\boldsymbol{f}(t, \boldsymbol{y}) = K\boldsymbol{y}$. In this case, it would be reasonable to use the following approximation to the solution $\boldsymbol{y}_n = \sum_j y_n^j \boldsymbol{v}^j$, where $\boldsymbol{v}^j$ are eigenvectors associated with eigenvalues λ^j in the generalised eigenvalue problem $M\boldsymbol{v} = \lambda K\boldsymbol{v}$. This means

that it is possible to deduce that $y_n^j = \mu_j^n y_0^j$ where in this particular case $\mu_j = \lambda^j/(\lambda^j - h)$. This gives a guideline on how to use a time step: in order to ensure the correct monotonic growth of the physical modes (growing on a time scale τ) in a qualitative sense we need to choose a time step h smaller than τ, or more precisely, h should be chosen smaller than the smallest positive τ^j. For quantitative accuracy, we note that $\mu = \exp(h/\tau) + O(h^2/\tau^2)$ which provide a criterion for choosing the value of h. Amongst other useful things (e.g., efficient storage), this procedure, which was proposed for the first time in [37] and extended in a straightforward manner to the general nonlinear case, ensures that inconsistent initial conditions will be resolved by the algorithm. Our higher order schemes can be interpreted through Romberg's extrapolation where, for example, for the second order schemes we use $\boldsymbol{y}_{n+1} = 2\hat{\boldsymbol{y}}_{n+1} - \bar{\boldsymbol{y}}_{n+1}$ with $\bar{\boldsymbol{y}}_{n+1}$ obtained with the one-step Euler's scheme, and $\hat{\boldsymbol{y}}_{n+1}$ obtained with two Euler's steps of length $h/2$ each. In a way similar to that explained above it can be shown that in this case the behaviour of the resulting scheme (which is the second order scheme as soon as h is small compared to τ) can be characterised by $\mu = \exp(h/\tau) + O(h^3/\tau^3)$ [37]. This idea is implemented in the general case in code called `dae2`. The total procedure is a three-level algorithm, and the other two levels, based on fourth-order accurate scheme `dae4` and multi-step method `dae40`, are used to confirm the result obtained with `dae2`. Note that the level `dae2` needs at least 2 steps for start-up, `dae4` needs at least 4, and `dae40` starts with three sub-steps. The `dae40` ensures resolving high oscillatory modes since it is constructed by dividing each step in the forth-order code `dae4` by three sub-steps. This, however, would require three times as large systems of linear equations compared to `dae4`.

As we mentioned above, the program requires a consistent initial condition $\mathtt{y0} \equiv \mathbf{y}_0$, but if the condition is not consistent the code automatically works towards consistency. In particular, having `y0` we find the backward differences to fit the initial data by making the first step *a multiple step*, and by requiring the unknown initial backward differences (stored in `yy`) suit all information across our multiple steps. After the Newton procedure determines the initial multistep, we perform the following steps of the algorithm [37]:

- we use the estimated backward differences at the initial time to extrapolate to each of the future time steps;
- by using these estimates of the function and its derivatives, we evaluate the residuals of the DAEs at each time (as well as the Jacobians at each of these times);
- we solve the simultaneous equations to find updates of the initial backward differences that would more accurately satisfy the DAEs at each of the times (if the Jacobian matrices are returned as sparse, the code will automatically switches on a quick sparse algorithm);
- we exit the loop if the updates to the backward differences at the initial time (stored in `yy`) are small enough relative to the overall magnitude of the variables and their differences.

The developed `MATLAB` code is simple, robust and easy to implement. It can be applied as soon as the original system for SMA dynamics is reduced to form $\tilde{\mathbf{f}}(\mathtt{t}, \mathbf{y}, \mathbf{y}') = \mathbf{0}$ with given vector function $\tilde{\mathbf{f}}$, and the integration procedure, starting from column-vector `y0` at time `t0` and finishing at time `tfin`, returns the solution at all times in $\mathtt{tspan} = [\mathtt{t0}, \mathtt{t1}, ..., \mathtt{tfin}]$. The time step and `tspan`, responsible for error management, and the Jacobian of $\tilde{\mathbf{f}}$ are provided by the user to compute $[\mathtt{f}, \mathtt{k}, \mathtt{m}] = \mathtt{func}(\mathtt{t}, \mathtt{y}, \mathtt{y}')$. As we explained above, both `k` and `m` may be given as sparse matrices, and our three-level procedure takes care of the convergence of the algorithm. For all computational experiments reported in the next section the first level of the algorithm with second-order accurate spatial differences on staggered grids (`dae2`) is sufficient.

7
Representative examples of computational experiments

The control of phase transitions in shape memory alloys and the quantification of hysteresis phenomena are topics of considerable interest [10]. By using several representative examples, in this section we demonstrate that our computational methodology is well suited to address these problems, being both simple and efficient.

We have applied our computational methodology to modelling a wide range of thermally and mechanically induced phase transitions. One of the problems important in many industrial applications is to describe quantitatively the stress-induced phase transition since such a transition may or may not exhibit a hysteresis behaviour, subject to thermodynamic barriers. In our computational examples we model these barriers by the boundary stress.

Consider a low-temperature regime (e.g., [1]) where we keep the rod in a martensitic state by imposing the initial thermal condition $\theta(x, 0) = 230$, and the initial mechanical conditions $u(x, 0) = kx$, $v(x, 0) = 0$. As an example, our rod is initially in the stable M_+ state with no distributed loading (we take $k = 0.106051$, $F = G = 0$). When thermomechanical conditions of the rod change, a phase transition can be induced. This can be modelled effectively with the computational methodology we have developed.

In a series of computational experiments we load the rod with a compressive load for some period of time $[0, t_1]$, then we apply a tensile load for another period of time $[t_2, t_3]$ (with $t_1 < t_2$), while keeping the stress at the boundaries constant outside of these two periods of time. More precisely, we impose the following mechanical boundary conditions

$$s = \begin{cases} A_1\omega(t), & 0 \le t < t_1, \\ A_2\omega(t), & t_2 \le t \le t_3, \\ A_3, & \text{otherwise} \end{cases}, \tag{32}$$

with no thermal flux conditions across the boundaries ($\partial\theta/\partial x = 0$). We choose function $\omega(t)$ in form $\sin^3(\pi t/6)$ (the physical units of s are $\mathrm{g}/(\mathrm{ms}^3\,\mathrm{cm})$) with constants A_i, $i = 1, 2, 3$ varying upon a specific situation. First we want to demonstrate that our computational methodology can deal with ease with $M_+ \to M_-$ phase transformations. As an example, we choose $A_1 = 7000$, $A_2 = -7000$, $A_3 = 0$, $t_1 = 6$, $t_2 = 12$, and $t_3 = 18$. Figure 4 (left) shows that the phase transformations $M_+ \to M_-$ are well reproduced with our code. We also observe the appearance of two upward and

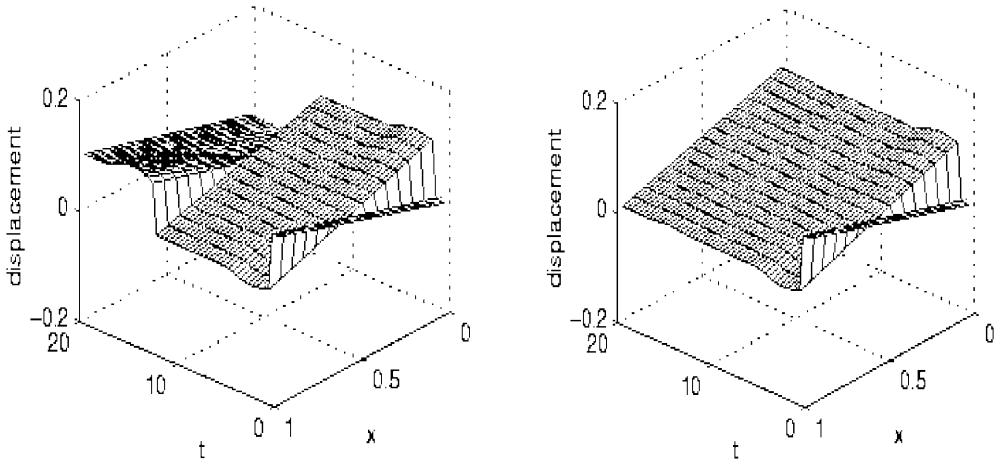

Fig. 4. Modelling stress-induced phase transitions: **a** tensile load exceeds the yield limit; **b** tensile load is less than the yield limit

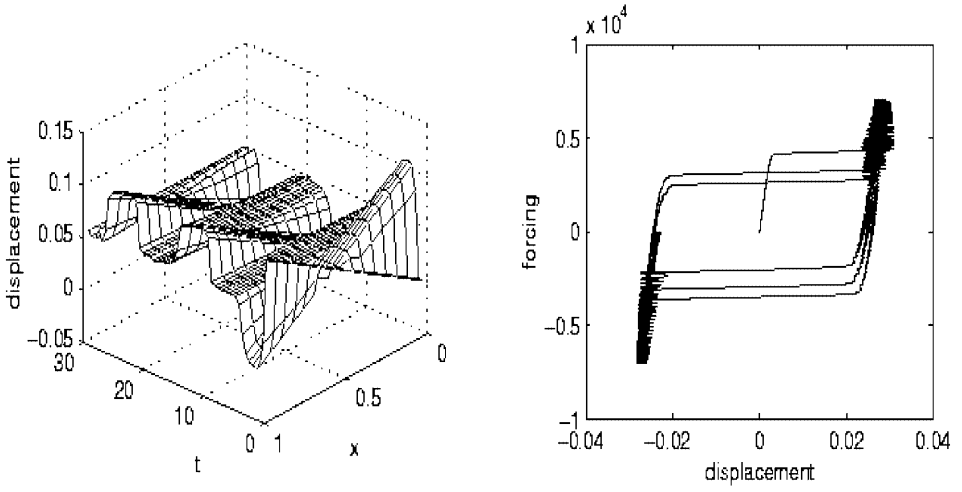

Fig. 5. **a** Modelling phase transitions with thermal control of thermodynamic barriers; **b** modelling hysteresis with load-deformation-type diagrams (the "ferroelastic" range of behaviour is shown

downward "humps" responsible for thermomechanical coupling effects between the two phases in the period when the temperature pattern changes. As expected, when time passes these regions vanish leaving only the M_- phase which is in stable equilibrium. Due to the tensile load applied, a reverse phase transformation $M_- \to M_+$ is also observed in Fig. 4 (left). Within this low-temperature regime, the material behaviour is rather similar to the behaviour of ferroelastics. As expected, no intermediate austenite phase under the above thermomechanical conditions was observed.

Note that as soon as the tensile loading is lower than the yield limit, we would expect that the sample remains in the M_- phase. This was observed in our computational experiment, as demonstrated by Fig. 4 (right) ($A_1 = 7000$, $A_2 = -700$, $A_3 = 0$). As we noted in [29] the situation will remain qualitatively the same for different constant load applied outside the times where the compressive or tensile loads are applied (e.g., take (32) as above but with any arbitrary value of A_3, say, between 0 and 100).

The "purely" mechanical control of phase transitions demonstrated above may not be always efficient, and the interest to "temperature-induced" phase transformations has increased dramatically over the recent years [5]. With the developed computational code we can model such transitions in SMA. Consider, for example, the previous problem where we were unable to return to the M_+ phase by "purely" mechanical means due to a low tensile load, and let us take $A_1 = 7000$, $A_2 = -700$, $A_3 = 100$. However, now we assume distributed heating/cooling changes according to the following rule $G = 375\omega(t)\,\mathrm{g}/(\mathrm{ms}^3\,\mathrm{cm})$. While, as we have seen, the mechanical load alone is not sufficient here to induce the phase transition, with this distributed thermal dynamics we can control the phase transition process effectively. A chain of transitions $M_+ \to M_- \to A \to M_+ \to A$ is demonstrated clearly in Fig. 5 (left).

Finally, we apply our methodology to modelling hysteresis loops. There is an increased interest in models for hysteresis from both theoretical (e.g., [42]) and practical (e.g., [4, 11, 12]) points of views, but to quantify hysteresis phenomena remains a formidable task. Models with hysteresis are used for the description of the dynamics of shape memory alloys where hysteresis phenomena can be represented by load-deformation diagrams (e.g., [9, 24]). Our last representative example shows that such diagrams can be obtained computationally with our code. Consider, for example, a normalise rod in a twin-martensite configuration defined by the following conditions

$$u^0 = \begin{cases} ax, & 0 \le x \le x_1, \\ a(0.5 - x), & x_1 \le x \le x_2, \\ a(x - 1), & x_2 \le x \le 1, \end{cases} \quad v^0 \equiv u^1 = 0. \tag{33}$$

We are interested in the low-temperature range, and take $\theta^0 = 220$ as our thermal initial condition. We take $a = 0.11869$, $x_1 = 0.25$, $x_2 = 0.75$ in (33), and assume pinned-end mechanical conditions $u = 0$, and no-flux thermal boundary conditions $\partial\theta/\partial x = 0$. Since we are within a "ferroelastic" range of behaviour of the SMA sample, when looking at load-deformation diagrams we expect a hysteresis-like behaviour (e.g., [9, 24]). This is clearly demonstrated by Fig. 5 (right) where we assumed that the thermal loading is absent ($G = 0$), and we took the distributed mechanical loading varying in time according to the rule $F = 7000\ \sin^3(\pi t/2)\ \mathrm{g}/(\mathrm{ms}^3\ \mathrm{cm})$. We plotted u as function of F at fixed spatial grid point $n_h = n/2 - 3$ where for the case presented $n = 16$.

The methodology developed here can be efficiently applied to high dimensional models as well, as soon as appropriate centre manifold models are derived, e.g. [28].

8
Concluding remarks

In this paper we derived a mathematical model for the description of SMA dynamics by using the Cattaneo–Vernotte law for heat conduction and accounting for nonlocal effects. We proposed a procedure for the reduction of models describing coupled thermodynamics of SMA materials to systems of differential-algebraic equations, and developed an efficient algorithm for the numerical solution of such systems. In the dimensions higher than one, approximations to models describing the dynamics of shape memory alloys can be systematically derived via the application of centre manifold theory [27, 28], and then the procedure developed here can be also applied.

All major effects observed in SMA materials, including pseudoelastic effect, shape memory effect, and thermal hysteresis, can be efficiently reproduced with our algorithms. It should be possible to extend the solution schemes developed in this paper to models in the finite-strain framework. Finally, we note that despite fantastic opportunities SMA materials can offer, they have a disadvantage of high response time. The speed of SMA materials can be increased by using the Peltier effect which was discussed in our previous paper [30]. The slow response time problem can also be overcome by developing SMA-based composites, thin SMA fibres and films [7]. It is believed that the algorithm developed in this paper can open new possibilities for more accurate modelling of martensitic transformations for these new materials.

References

1. **Alt HW, Hoffmann K-H, Niezgodka M, Sprekels J** (1985) A Numerical Study of Structural Phase Transitions in Shape Memory Alloys. Department of Mathematics, University of Augsburg, vol. 90
2. **Auricchio F, Taylor RL** (1999) A return-map algorithm for general associative isotropic elasto-plastic materials in large deformation regimes. Int. J. Placticity 15: 1359–1378
3. **Balta F, Suhubi ES** (1977) Theory of Nonlocal Generalised Thermoelasticity. Int. J. Eng. Sci. 15: 579–588
4. **Bank H-T et al.** (1999) Modeling of nonlinear hysteresis in elastomers under uniaxial tension. J. Intel. Material Syst. Struct. 10: 116–134
5. **Bekker A, Brinson LC** (1997) Temperature-induced phase transformation in a shape memory alloy: phase diagram based kinetics approach. J. Mech. Phys. Solids 45: 949–988
6. **Benzaoui H et al.** (1997) Experimental study and modelling of a TiNi shape memory alloy wire actuator. J. Intell. Material Syst. Struct. 8: 619–629
7. **Bidaux JE, Yu WJ, Gotthardt R, Manson JAE** (1995) Modelling of the martensitic transformation in SMA composites. J. de Physique IV C2(5): 543–548
8. **Birman V** (1997) Review of mechanics of shape memory alloy structures. Appl. Mech. Rev. 50: 629–645
9. **Bornert M, Muller I** (1990) Temperature dependence of hysteresis in pseudoelasticity. In: Hoffmann K-H, Sprekels J (eds) Free Boundary Value Problems, Birkhauser pp 27–35
10. **Bubner N, Sokolowski J, Sprekels J** (1998) Optimal boundary control problems for shape memory alloys under state constraints for stress and temperature. Numer. Funct. Anal. Optimiz. 19: 489–498
11. **Bubner N, Mackin G, Rogers R** (2000) Rate dependence of hysteresis in one-dimensional phase transitions. Comput. Materials Sci. 18: 245–254
12. **Bubner N** (1996) Landau-Ginzburg model for a deformation-driven experiment on shape memory alloys. Continuum Mech. Thermodyn. 8: 293–308
13. **Chen Z, Hoffmann K-H** (1994) On a one-dimensional nonlinear thermoviscoelastic model for structural phase transitions in shape memory alloys. J. Differential Equations 112: 325–350
14. **Colli P, Grasselli M** (1995) Justification of a hyperbolic approach to phase changes in materials with Memory. Asymptotic Anal. 10: 303–334
15. **DeGiorgi VG, Saleem H** (1999) A comparison of a few SMA constitutive models. SPIE Proceedings 3667: 3667–3678
16. **Falk F** (1980) Model free energy, mechanics, and thermomechanics of shape memory alloys. Acta Metallurgica 28: 1773–1780
17. **Falk F, Konopka P** (1990) Three-dimensional Landau theory describing the martensitic phase transformation of shape-memory alloys. J. Phys.: Condens. Matter. 2: 61–77
18. **Feehery WF, Tolsma JE, Barton PI** (1997) Efficient sensitivity analysis of large-scale differential-algebraic systems. Appl. Numer. Math. 25(1): 41–54
19. **Gobbert MK, Prohl A** (1999) A discontinuous finite element method for solving a multi-well problem. SIAM J. Numer. Anal. 37(1): 246–268
20. **Hoffmann K-H, Niezgodka M, Songmu Z** (1990) Existence and uniqueness of global solutions to an extended model of the dynamic developments in SMA. Nonlinear Analysis: TMA 15(10): 977–990
21. **Hoffmann KH, Niezgodka M** (1990) Mathematical models of dynamical martensitic transformations in shape memory alloys. J. Intell. Mater. Syst. Struct 1: 355–374
22. **Hoffmann K-H, Zou J** (1995) Finite element approximations of Landau-Ginzburg's equation model for structural phase transitions in shape memory alloys. M^2AN 29(6): 629–655
23. **Huo Y, Muller I, Seelecke S** (1994) Quasiplasticity and pseudoelasticity in shape memory alloys. Phase Transitions and Hysteresis, Brokate M et al. (eds) Springer-Verlag, pp 87–146
24. **Klein O** (1995) Stability and uniqueness results for a numerical approximation of the thermomechanical phase transitions in shape memory alloys. Adv. Math. Sci. Appl. (Tokyo), 5(1): 91–116
25. **Li B, Luskin M** (1998) Finite element analysis of microstructure from the cubic to tetragonal transformation. SIAM J. Numer. Anal 35(1): 376–392
26. **Maugin GA** (1999) Nonlinear Waves in Elastic Crystals. Oxford University Press, Oxford, NY

27. **Melnik RVN, Roberts AJ, Thomas KA** (2000) Mathematical and numerical analysis of Falk–Konopka-type models for shape memory alloys. Int. J. Differential Equations Appl. 1A(3): 291–300
28. **Melnik RVN, Roberts AJ, Thomas KA** (2000) Computing dynamics of copper-based SMA via centre manifold reduction of 3D models. Comput. Materials Sci. 18: 255–268
29. **Melnik RVN, Roberts AJ, Thomas KA** (2001) Coupled thermomechanical dynamics of phase transitions in shape memory alloys and related hysteresis phenomena. Mechanics Research Communications 28(6): 637–651
30. **Melnik RVN, Roberts AJ** (2001) Thermomechanical behaviour of thermoelectric SMA actuators. Journal de Physique IV 88(8): 515–520
31. **Moyne S, Boubakar ML, Lexcellent C** (1997) Extension of a linear behaviour model of SMA for finite strain studies. J. Phys. IV France, Colloque C5 7: 83–88
32. **Muller I, Ruggeri T** (1993) Extended Thermodynamics. Springer-Verlag
33. **Niezgodka M, Sprekels J** (1991) Convergent numerical approximations of the thermomechanical phase transitions in shape memory alloys. Numer. Math 58: 759–778
34. **Pawlow I** (2000) 3D model of thermomechanical evolution of shape memory materials. Control and Cybernetics 29(1): 341–365
35. **Renardy M, Hrusa WJ, Nohel JA** (1987) Mathematical Problems in Viscoelasticity. Longman Scientific & Technical
36. **Roberts AJ** (1997) Low-dimensional modelling of dynamics via computer algebra. Comp. Phys. Commun. 100: 215–230
37. **Roberts AJ** (2001) Solve differential-algebraic equations in MATLAB, `http://www.sci.usq.edu.au`
38. **Souza AC, Mamiya EN, Zouain N** (1998) A new 3D constitutive model for SMA. In: Idelsohn S, Onate E, Dvorkin E (eds) Computational Mechanics: New Trends and Applications. CIMNE, Barcelona, Spain
39. **Sprekels J** (1989) Global existence for thermomechanical processes with nonconvex free energies of Ginzburg–Landau form. J. Mathematical Anal. Appl. 141: 333–348
40. **Sprekels J** (1990) Shape memory alloys: mathematical models for a class of first order solid–solid phase transitions in metals. Control and Cybernetics 19(3–4): 287–308
41. **Strunin DV, Melnik RVN, Roberts AJ** (2001) Coupled thermomechanical waves in hyperbolic thermoelasticity. J. Thermal Stresses 24(2): 121–140
42. **Visintin A** (2001) Hyperbolic equations with hysteresis. C.R. Acad. Sci. Paris, Series I 332: 315–320